Proceedings of the Korean Nuclear Society Spring Meeting
Kwangju, Korea, May 2002

Analysis of External Reactor Vessel Cooling with COASISO During a Core Melt Accident

Chan Soo Kim, Kune Y. Suh*, Goon C. Park, Un C. Lee

Seoul National University
San 56-1, Sillim-Dong, Kwanak-Gu, Seoul, 151-742, Korea
*Phone: +82-2-880-8324, Fax: +82-2-889-2688, Email: kysuh@snu.ac.kr

Abstract

As an IVR-EVC (In-Vessel Retention through External Vessel Cooling) design concept, external cooling of the reactor vessel was suggested to protect the lower head from being overheated due to relocated material from the core during a severe accident. COASISO (Corium Attack Syndrome Immunization Structures Outside the vessel) is an external vessel cooling strategy by flooding inside the thermal insulator. Its advantage is the quick response time so that the initial heat removal mechanism of the EVC is nucleate boiling from the downward-facing lower head. The efficiency of the COASISO may be estimated by the thermal margin defined as the ratio of the actual heat flux from the reactor vessel to the critical heat flux (CHF). In this study the thermal margin for the large power reactor as the APR1400 (Advanced Power Reactor 1400 MWe) was determined by means of transient analysis for the local condition of the coolant and temperature distributions within the reactor vessel. The heat split fraction in the oxide pool and the metal layer focusing effect were considered for calculation of the angular thermal load at the inner wall of the lower head. The temperature distributions of the reactor vessel resulted in the actual heat flux on the outer wall. The local quality was obtained by solving the simplified transient energy equation. The unheated section of the reactor vessel decreases the thermal margin by mean of the two-dimensional conduction heat transfer. The peak temperature of the reactor vessel was estimated in the film boiling region as the thermal margin was equal to 1. Sensitivity analyses were performed for the time of corium relocation after the reactor trip, the coolant flow rate, and the initial subcooled condition of the coolant. This methodology will be implemented into the severe accident analysis code MAAP4 for the external vessel cooling with the COASISO.

1. Introduction

A wide spectrum of management strategies have so far been proposed to cope with nuclear

reactor severe accident. As a viable means to ensure adequate cooling of the decay heat generating debris bed and the vessel wall, the so-called IVR-EVC (in-vessel retention through external vessel cooling) appears to draw a keen attention from the nuclear safety community. Quite recently the COASISO (Corium Attack Syndrome Immunization Structure Outside the vessel) is being developed at the Seoul National University as a prospective in-vessel retention device for a next-generation water reactor in concert with existing ex-vessel management measures [1]. As quantitative analysis as may reasonably be performed is prerequisite to estimating the thermal and mechanical margins of the reactor vessel wall containing the exceedingly high temperature core material when the IVR-EVC design is considered in the next-generation reactors as well as already operating nuclear power plants. But the effect on the thermal margin of the local transient condition of the external coolant was taken into account in previous studies. All the calculations in this study were performed to estimate the effect of the transient local condition of the external coolant and the cylindrical part of the reactor vessel on the thermal margin.

Yoon and Suh [2] estimated the efficiency of the external vessel cooling by the thermal margin in terms of the critical heat flux ratio (CHFR) as the ratio of the CHF to the actual heat flux from the reactor vessel. The CHF was calculated by Cheung et al's model [3]. The forced convection effect was rather roughly considered by slightly modifying the former model. Their results indicated the higher thermal margin at the bottom region because more heat was being transferred to the top region relative to the bottom region by means of the natural convection effect in the molten pool. The results also showed that more heat could be removed by forced convection and subcooled boiling versus natural convection and saturated boiling.

Kim and Suh [4] also estimated the efficiency of the external vessel cooling per the CHFR. The CHF was calculated from Rouge et al.'s correlation [5] utilizing the postulated local condition. Their results indicated a higher thermal margin at the bottom than at the top of the vessel on account of the natural convection taking place within the hemispherical molten debris pool in the lower plenum. The information obtained from this study served to identify the maximum heat removal capability and limitations of the IVR-EVC technology called the COASISO.

Park and Jeong [6] calculated the thermal margin for the external reactor vessel cooling in a large advanced light water reactor (ALWR). They chose Steinberner and Reineke's Nusselt (Nu) number [7] for the upward natural convection and Theofanous et al's Nu [8] for the downward convection, respectively. They also cited the correlation based on the Mini-ACOPO experimental data to find the angular heat flux distribution and obtained the CHF at the outer surface of the lower head using Theofanous et al.'s correlation [8] developed from the experimental data of ULPU-2000 configuration II. Their results showed that the thermal margins were 1.27 and 1.64 depending on which correlation was used at the highest angle of the debris, i.e. θ=85o measured from the bottom of the vessel.

Theofanous et al. [8] estimated the integrity of the vessel during severe accident by experiments on the natural convection in the molten pool and the CHF on the outer vessel wall. Thermal and mechanical analyses of the reactor vessel were carried out particularly concerning the metal layer focusing effect.

Park and Dhir [9] investigated the effectiveness of flooding the cavity of a pressurized water reactor (PWR) in preventing vessel melt-through in case of melting and relocation of

the core material in the vessel lower head. Two-dimensional transient and steady-state analyses were carried out including heat loss by radiation to the upper regions of the reactor vessel and the unwetted portion of the vessel lower head. The effect of internal circulation in the molten core material on heat transfer at the bounding walls was determined by extending the correlations used in their study. Radiative heat transfer from the molten pool to the surrounding structures was also included in the analysis.

O'Brien and Hawkes [10] performed a thermal analysis to assess the viability of external water flooding as a cooling strategy to prevent the reactor vessel thermal failure in case of a severe accident with partial core melting and relocation to the reactor vessel lower head. For the molten pool in the reactor vessel lower head, the turbulent natural convection heat flux distribution predicted from the FIDAP simulation was used to determine the vessel wall temperature. Vessel wall temperatures and heat fluxes were obtained over a range of decay heating values using a one-dimensional heat conduction model. It was concluded that thermal failure of the vessel wall would occur if the turbulent natural convection heat transfer coefficients predicted from the numerical simulation were correct.

Henry and Fauske [11] performed the experiment to demonstrate that nucleate boiling is the dominant heat removal process from the outer surface of a simulated reactor vessel lower head surrounded by typical reflective insulator. Their experiment indicated that heat fluxes approaching 1MW/m2 could be removed by boiling on the outer surface even with the vessel insulated. No indications of high wall surface temperatures were measured. They insisted that the entire transient was characterized by nuclear boiling and the reactor vessel lower head would be able to effectively remove the energy transferred to the vessel wall through the debris crust.

Kim and Jin [12] performed the temperature and stress analyses for core melting accident by using the ABAQUS code. They discussed the potential for vessel damage using the Larson-Miller curve and damage rule. They also compared the results of transient analysis.

2. Model Description

Figure 1 schematically shows the hemispherical shell structure COASISO for heat removal from the reactor vessel lower head considered mainly and uniquely in this study in assessing the IVR capability.

The basic factors influencing the thermal margin calculation are the amount of heat to be transferred downward from the debris pool, the angular variation of local heat flux on the downward surface, transient conduction heat transfer in the reactor vessel, and the amount of removable heat by the external vessel cooling. The first two factors arise from the natural convection within the molten pool of debris, the metal layer focusing effect, and the amount of the corium while the last factor results from the heat removal capability of the injected water outside the reactor vessel lower head.

Table 1 presents the selected correlations in this study. The sensitivity analysis on the thermal margin is performed about the time of corium relocation, the external coolant flow rate, and the initial subcooled condition. Figure 2 illustrates the flow diagram for the transient analysis in this study.convection heat flux distribution predicted from the FIDAP simulation was used to determine the vessel wall temperature. Vessel wall temperatures and heat fluxes

were obtained over a range of decay heating values using a one-dimensional heat conduction model. It was concluded that thermal failure of the vessel wall would occur if the turbulent natural convection heat transfer coefficients predicted from the numerical simulation were correct.

2.1.Thermal Load

To estimate the thermal margin, the amount of heat transferred to the vessel from the internal pool must be determined a priori. Quite a few assumptions are necessary to facilitate the calculation. The amount of heat source is determined from the decay heat and the mass fraction of the relocated corium. It is assumed that decay heat led to the melt progression and relocation of the homogenous mixture of corium without heat removal in the core. The transient decay heat in the molten pool is transported to the surroundings without any storage of heat. The crust effect is not taken into account in this study.

In this study 1 hr, 1.5 hr, and 2 hr after the reactor shutdown were selected as the time of corium relocation. Figure 3 demonstrates varying decay heat profiles pursuant to the time of core relocation. The decay power may be expressed as referenced in El-Wakil [14]

$$Q_{decay} = Q_{steady} \times 0.095 \times \left(time_s + time\right)^{-0.26} \tag{1}$$

Given the decay power, the mass of relocated corium may be determined from

$$\dot{m}_{rel} = Q_{decay} \frac{M_{corium} - M_{rel}}{M_{corium}} \tag{2}$$

After all the corium is relocated in the lower head it is assumed that stratification of the oxidic pool and the metal layer takes place immediately. When all the corium is relocated to the lower head, the angle of the total, i.e. oxidic and metallic, corium pool is 84 degrees. The angle of the oxidic pool is 76 degrees. The material properties of the corium are referenced from Park and Dhir [9]. The material properties of the oxidic pool and the metal layer are referenced from Park and Jeong [6].

To examine the amount of heat transferred downward due to natural convection in the oxidic pool or the corium pool, correlations were developed with modified Rayleigh number (Ra'). Ra' is normally defined as

$$Ra' = \frac{g\beta_p Q_V H_p^{\,5}}{k_p \alpha_p \nu_p} \tag{3}$$

A wide spectrum of data were taken from different geometries of rectangular, semicircular, hemispherical and torispherical pool. Some of the data were obtained from experiments while the other data were derived from numerical studies. Theofanous et al.'s correlation [12] is selected because their experiment ACOPO's geometry was the hemisphere of the actual diameter. Utilizing the natural convection correlation for the downward versus the upward heat transfer, the heat split fraction was calculated as

$$frac = \frac{Nu_{down} A_{down}}{Nu_{down} A_{downn} + Nu_{up} A_{up}} \tag{4}$$

For all the experimental studies carried out so far it was assumed that the heat flux from the debris bed to the vessel wall varies azimuthally. For years a number of investigators have

studied the heat flux from the debris to the reactor vessel lower head. They concentrated on several natural convection experiments in the lower head vessel. In this study we chose Theofanous et al.'s correlation [8] for the heat transfer coefficient varying with the local position.

$$q''_{down} = Q_{decay} \frac{M_{rel}}{M_{corium}} \left(A_{down}\right)^{-1} \tag{5}$$

$$\begin{aligned} q''(\theta)/q''_{down} &= 0.1 + 1.08\left(\theta/\theta_p\right) - 4.5\left(\theta/\theta_p\right)^2 + 8.6\left(\theta/\theta_p\right)^3 \\ &\quad for \quad 0.1 < \theta/\theta_p \le 0.6 \\ q''(\theta)/q''_{down} &= 0.41 + 0.35\left(\theta/\theta_p\right) + \left(\theta/\theta_p\right)^2 \\ &\quad for \quad 0.6 < \theta/\theta_p \le 1 \end{aligned} \tag{6}$$

The metal layer focusing effect is estimated by means of the three energy balances. For the energy balance of the metal layer, the following assumptions are made to simplify the energy equations:

(1) constant side boundary temperature: melting point of metal layer: 1600oC,

(2) the same material properties in all the region of the metal layer,

(3) the negligible crust thickness between the oxide pool and the metal layer, and

(4) only the radiation heat transfer mechanism on the upper surface to the external region.

Based on the above assumptions the heat transferred upward from the oxide pool is equal to the heat convected from the oxide pool transmitted to the metal layer. It is also equal to the sum of the heat transferred to the upper surface and the heat transfer to the wall. The heat transferred to the upper surface is the same as the radiation heat transfer from the upper surface. The energy balances in the metal layer can be described as the following three equations [8].

$$Q_{decay}\left(1 - frac\right) = h_{12}A_{12}\left(T_{12} - T_2\right) \tag{7}$$

$$h_{12}A_{12}\left(T_{12} - T_2\right) = h_{2w}A_{2w}\left(T_2 - T_{2w}\right) + h_{23}A_{23}\left(T_2 - T_{23}\right) \tag{8}$$

$$h_{23}A_{23}\left(T_{12} - T_2\right) = \varepsilon\sigma T_{23}^4 \tag{9}$$

The convective heat transfer coefficient is applied from the Globe-Dropkin's equation [15].

$$Nu = 0.059 Ra^{1/3} \tag{10}$$

The temperatures of the metal layer are taken from Equations (7), (8) and (9). The actual heat flux from the metal layer to the vessel wall can be obtained as follows:

$$q''_{2w} = h_{2w}\left(T_2 - T_{2w}\right) \tag{11}$$

Figure 4 shows the flow diagram for obtaining the thermal load with the metal layer focusing effect.

2.2. Two Dimensional Conduction Heat Transfer

In calculating the two-dimensional temperature profile in the vessel for the external and no external cooling cases we used the alternating direction implicit (ADI) method taken from El-Genk and Cao [16] and Yoon and Suh [17] for the hemispherical and cylindrical geometries. This method calculates the temperature implicitly alternating in r and θ or z directions,

respectively, as

$$\rho c_p\left(\frac{\partial T}{\partial t}\right)=\frac{1}{r^2}\frac{\partial}{\partial r}\left(kr^2\frac{\partial T}{\partial r}\right)+\frac{1}{r^2\sin\theta}\frac{\partial}{\partial\theta}\left(k\sin\theta\frac{\partial T}{\partial\theta}\right) \tag{12}$$

$$\rho c_p\left(\frac{\partial T}{\partial t}\right)=\frac{1}{r}\frac{\partial}{\partial r}\left(kr\frac{\partial T}{\partial r}\right)+\frac{\partial}{\partial z}\left(k\frac{\partial T}{\partial z}\right) \tag{13}$$

The diffusion terms of Equations (12) and (13) are discretized and split into two parts. The whole solution is obtained in two steps. In the first step the diffusion terms in the θ or z direction are represented implicitly, while those in the r direction are explicit:

$$\begin{aligned}\rho_v c_{p_v}\Delta V_{i,j}\frac{T^*_{i,j}-T^n_{i,j}}{\Delta t/2}&=k_{v\,i,j}^{\;L}\frac{T^*_{i,j-1}-T^*_{i,j}}{r_i\Delta\theta}\Delta AL^v_{i,j}+k_{v\,i,j}^{\;R}\frac{T^*_{i,j+1}-T^*_{i,j}}{r_i\Delta\theta}\Delta AR^v_{i,j}\\&+k_{v\,i,j}^{\;U}\frac{T^n_{i+1,j}-T^n_{i,j}}{\Delta r}\Delta AU^v_{i,j}+k_{v\,i,j}^{\;D}\frac{T^n_{i-1,j}-T^n_{i,j}}{\Delta r}\Delta AD^v_{i,j}\end{aligned} \tag{14}$$

$$\begin{aligned}\rho_v c_{p_v}\Delta V_{i,j}\frac{T^*_{i,j}-T^n_{i,j}}{\Delta t/2}&=k_{v\,i,j}^{\;L}\frac{T^*_{i,j-1}-T^*_{i,j}}{\Delta z}\Delta AL^v_{i,j}+k_{v\,i,j}^{\;R}\frac{T^*_{i,j+1}-T^*_{i,j}}{\Delta z}\Delta AR^v_{i,j}\\&+k_{v\,i,j}^{\;U}\frac{T^n_{i+1,j}-T^n_{i,j}}{\Delta r}\Delta AU^v_{i,j}+k_{v\,i,j}^{\;D}\frac{T^n_{i-1,j}-T^n_{i,j}}{\Delta r}\Delta AD^v_{i,j}\end{aligned} \tag{15}$$

In the second step, the diffusion terms in the θ or z direction are represented explicitly, while those in the r direction are implicit:

$$\begin{aligned}\rho_v c_{p_v}\Delta V_{i,j}\frac{T^{n+1}_{i,j}-T^*_{i,j}}{\Delta t/2}&=k_{v\,i,j}^{\;L}\frac{T^*_{i,j-1}-T^*_{i,j}}{r_i\Delta\theta}\Delta AL^v_{i,j}+k_{v\,i,j}^{\;R}\frac{T^*_{i,j+1}-T^*_{i,j}}{r_i\Delta\theta}\Delta AR^v_{i,j}\\&+k_{v\,i,j}^{\;U}\frac{T^{n+1}_{i+1,j}-T^{n+1}_{i,j}}{\Delta r}\Delta AU^v_{i,j}+k_{v\,i,j}^{\;D}\frac{T^{n+1}_{i-1,j}-T^{n+1}_{i,j}}{\Delta r}\Delta AD^v_{i,j}\end{aligned} \tag{16}$$

$$\begin{aligned}\rho_v c_{p_v}\Delta V_{i,j}\frac{T^{n+1}_{i,j}-T^*_{i,j}}{\Delta t/2}&=k_{v\,i,j}^{\;L}\frac{T^*_{i,j-1}-T^*_{i,j}}{\Delta z}\Delta AL^v_{i,j}+k_{v\,i,j}^{\;R}\frac{T^*_{i,j+1}-T^*_{i,j}}{\Delta z}\Delta AR^v_{i,j}\\&+k_{v\,i,j}^{\;U}\frac{T^{n+1}_{i+1,j}-T^{n+1}_{i,j}}{\Delta r}\Delta AU^v_{i,j}+k_{v\,i,j}^{\;D}\frac{T^{n+1}_{i-1,j}-T^{n+1}_{i,j}}{\Delta r}\Delta AD^v_{i,j}\end{aligned} \tag{17}$$

where T^n and T^{n+1} are the temperatures at the previous and present time steps, respectively, and T^* is the intermediate value. All the material properties of the vessel are taken from Stickler et al. [18]. The inner and the outer radii of the vessel are 2.35 m and 2.5 m, respectively, referring to the APR1400.

2.3. External Vessel Cooling

In the previous studies about the integrity of the reactor vessel, the CHF was dependent on only the angular position. The heat transfer coefficient on the outer surface was dependent on the angular position and on the wall superheat. Cheung and Liu [19] analyzed the upward co-current flow induced by the natural convection boiling process. Kim and Suh [4] argued that the local quality has the major effect on the CHF for the external cooling at the top. Because

the effect of the subcooling on the CHF was not explicitly considered in Rouge et al.'s correlation [5], the constant pressure condition is assumed in this study. Thus the single mass velocity model is applied in this study to calculate the transient local quality at angular positions.

The transient local quality can be obtained by solving the following transient energy equation

$$\rho_{ex}\left(\frac{\partial i}{\partial t}\right)+G_{ex}\frac{\partial i}{\partial z}=q''_{out}\frac{A_{heat}}{V_{ex}} \tag{18}$$

The volume integral form of Equation (18) is given by

$$\rho_j V_j \frac{i_{j+1}^{n+1}-i_j^n}{\Delta t}+\dot{m}\left(i_{j+1}^{n+1}-i_j^{n+1}\right)=q''_{out}A_{heat} \tag{19}$$

The uniform gap size between the COASISO shell structure and the reactor vessel is assumed to be 15 cm. It is assumed that the quality in the subcooled region is zero. The coolant mass flow rates are 20, 30, 40 and 50 kg/s. The initial subcooled condition of the external coolant is 60°C and the pressure is uniform at 0.12 MPa.

Rouge et al.'s correlation was based on the 191 CHF data from the SULTAN facility. The correlation included the local quality (x), gap (e) in m, pressure (p) in MPa, heat flux in MW/m^2, mass flux (G) in kg/m^{2}s, and inclination angle(θ) measured from the horizontal line

$$\begin{aligned}
q''_{CHF} &= A0(e,p,G)+A1(e,G)x+A2(e,p,G,x)x^2 \\
&\quad +A3(e,p,G,x)\sin\theta+A4(e,p,G,x)\sin^2\theta \\
A0 &= b0+b1\times e\times\ln G+b2/p^2+b3\times G+b4\times e/p+b5\times e/p^2+b6\times p\times(\ln G)^2 \\
A1 &= b7\times(\ln G)^2+b8\times e\times\ln G, \quad A2=b9\times e \\
A3 &= b10\times(\ln G)^2+b11\times e\times p+b12\times x\times\ln G \\
A4 &= b13\times p+b14\times\ln G+b15\times x+b16\times e \\
b0 &= 0.65444,\ b1=-1.2018,\ b2=-0.008388,\ b3=0.000179,\ b4=1.36899 \\
b5 &= -0.077415,\ b6=0.024967,\ b7=-0.086511,\ b8=-4.49425 \\
b9 &= 9.28489,\ b10=-0.0066169,\ b11=11.62546,\ b12=0.855759 \\
b13 &= -1.74177,\ b14=0.182895,\ b15=-1.8898,\ b16=2.2636
\end{aligned} \tag{20}$$

The CHF is calculated from the postulated local condition using the transient energy equation and the assumptions about the external cooling. The thermal margin is defined as the actual heat flux over the CHF at the angular position. The actual heat flux on the outer surface is expressed as

$$q''_{out}=h_j\left(T_j^{out}-T_b\right) \tag{21}$$

The film boiling heat transfer coefficient on the outer wall is referenced from Park and Dhir [9]. Because the wall superheat at the CHF is assumed as 70oC referenced from Cheung and Liu [19], the nucleate boiling heat transfer coefficient is defined as

$$h_j = \frac{q''_{CHF}}{70} \tag{22}$$

The local heat transfer coefficient is determined by the method as illustrated in Figure 5.

3. Results and Discussion

Figure 6 shows the corium pool angle differing the time of corium relocation after the reactor trip. The later start time of corium relocation delays the complete relocation of corium. Figure 7 shows that Ra' for the decay heat generating pool. The sudden reduction of Ra' results from the instantaneous shrinkage of the volumetrically heated pool height due to stratification of the oxidic pool and the metal layer in the reactor lower head.

Figure 8 shows the downward heat split fraction of the volumetrically heated oxidic or corium pool. From the modified Rayleigh number of Figure 7 the downward heat split fraction has the large value in the high Ra' because of the large downward heated area. Sudden reduction of the fraction is due to the reduction of the pool height by the sudden reduction of volumetrically heated pool height accounting for stratification of the oxidic pool and the metal layer in the reactor lower head.

Figure 9 presents the angular distribution of the thermal load on the inner wall at the earlier phase. The sudden increase of heat flux occurs at the bottom because of the unstable region in the molten pool. But the heat flux decreases sharply when the molten pool is large enough to attain stability. When the region is unstable, there is no steep decrease of the heat flux. Figures 10 and 11 demonstrate the angular distribution of the thermal load on the inner wall and the actual heat flux on the outer wall in case 342. In particular the thermal load at the top is suddenly increased, but the actual heat flux is not suddenly increased as the thermal load due to the sensible and latent heat of the reactor vessel. The heat flux on the inner wall is zero, but that on the outer wall is not zero at 85o because of the two-dimensional conduction heat transfer effect.

Figure 12 shows the angular minimum CHF distribution in the eight cases of the external vessel cooling. There is no difference in the minimum CHF with time of the corium relocation after reactor trip. Figures 13 and 14 present the history of the CHF at 80o with eight cases of the external cooling, when the time of corium relocation after reactor trip is 1.0 hr. According to Kim and Suh [4], the local thermodynamic quality has a decreasing effect on the CHF at the top unless the limiting value is reached above which the CHF may abruptly decrease. So the minimum CHF is smaller than the actual heat flux in several cases, though the initial CHF is larger than the maximum actual heat flux at all the angular positions. After sudden decrease in the CHF a little bit of increase in the CHF is due to decrease of the local quality and the actual heat flux by the transition from nucleate to film boiling in case where the vessel failure occurs.

Figure 15 depicts the maximum temperature of the outer surface for all the cases studied. When the thermal margin is 1.0 the vessel fails. The early start time of the corium relocation after reactor trip requires larger mass flow rate and initial subcooled condition of the external coolant.

4. Conclusion

In this study transient analyses were performed by means of the natural convection of the molten pool, transient two-dimensional conduction equation, and transient energy equation for the external vessel cooling. The required mass flow rate of the coolant and initial subcooled condition is estimated to maintain the vessel integrity with differing start time of corium relocation. Results of this study indicate that the relocation time is a pivotal factor in evaluating the in-vessel retention strategy. Sufficient mass flow rate and initial subcooled condition are required to maintain the general CHF of 1.5 MW/m2 at the top. So, the natural circulation flow rate of the coolant must be precisely estimated in the cavity flooding system selected as the external vessel cooling strategy of the APR1400. The two-dimensional conduction at the unheated zone decreases the actual heat flux at the top. In the future, the difference between the single mass velocity and momentum integral methods will be estimated for the external cooling. The heat split fraction will be obtained from the correlations with Ra based on the temperature difference in the molten pool. Finally, this computational scheme will be incorporated in the severe accident analysis code MAAP4 for external cooling utilizing the COASISO gap cooling structure.

NOMENCLATURE

A	area
AD	lower surface of the control volume
AL	left surface of the control volume
AR	right surface of the control volume
AU	upper surface of the control volume
c_p	specific heat
$frac$	downward heat split fraction
G	mass flux
g	gravity
H	pool height
h	heat transfer coefficient
i	enthalpy of the external vessel cooling coolant
k	thermal conductivity
M_{corium}	total mass of corium
M_{rel}	mass of relocated corium
$\dot{m}$	mass flow rate of coolant
$\dot{m}_{rel}$	mass velocity of corium relocation
Nu	Nusselt number
Q_{decay}	decay power
Q_{steady}	operating power
Q_V	volumetric heat generation rate
q''	heat flux
r	radial coordinate
Ra	Rayleigh number
Ra'	modified Rayleigh number
T	temperature
t	time
$time$	time after the start of corium relocation
$time_s$	the start time of corium relocation after reactor trip
V	volume of the control volume
z	axial coordinate

Greek Letters

α	thermal diffusivity
β	volumetric thermal expansion coefficient
Δ	finite increment
ν	kinematic viscosity
θ	angle, angular coordinate
ρ	density

Subscripts

12	the interface between oxidic pool and metal layer
$2w$	the interface between metal layer and vessel wall
2	metal layer

23	the top of metal layer
b	bulk
ex	external vessel cooling coolant
down	downward of volumetric heat generated pool
heat	heated area
i	radial node
j	angular and axial node
out	outer wall
p	volumetric heat generated pool
up	upward of volumetric heat generated pool
v	reactor vessel

Superscripts

n	previous time step
$n+1$	present time step
out	outer wall
v	reactor vessel
*	intermediate time step

References

1. I.S. Hwang, K.Y. Suh, "Gap Structure for Nuclear Reactor Vessel," United States Patent US 6,195,405 B1 (2001).
2. H.J. Yoon, K.Y. Suh, “Sensitivity Studies on Thermal Margin of Reactor Vessel Lower Head during a Core Melt Accident,” Proceedings of the 8th International Conference on Nuclear Engineering (ICONE-8), Baltimore, MD, USA (2000).
3. F.B. Cheung, K.H. Haddad, Y.C. Liu, Critical Heat Flux Phenomenon on a Downward Facing Curved Surface, NUREG/CR-6507 PSU/ME-7321 (1997).
4. C.S. Kim, K.Y. Suh, “Sensitivity Studies on Thermal Margin of Reactor Vessel Lower Head during a Core Melt Accident,” Journal of the Korean Nuclear Society, vol. 32, no. 4, p. 379 (2000)
5. S. Rouge, I. Dor, G. Geffraye, “Reactor Vessel External Cooling for Corium Retention SULTAN Experimental Program and Modeling with CATHARE Code,” Workshop on In-Vessel Core Debris Retention and Coolability, Garching, Germany (1998).
6. J.W. Park, D.W. Jeong, “An Investigation of Thermal Margin for External Reactor Vessel Cooling (ERVC) in Large Advanced Light Water Reactor (ALWR),” Proceedings of the Korean Nuclear Society Spring Meeting, p. 473, Seoul, Korea (1997).
7. U. Steinberner, H.H. Reineke, “Turbulent Buoyancy Convection Heat Transfer with Internal Heat Source,: Proceeding 6th International Heat Transfer Conference, Toronto, Canada (1978).
8. T.G. Theofanous, C. Liu, S. Additon, S. Angelini, O. Kymalainen, T. Salmassi, In-vessel Coolability and Retention of a Core Melt, DOE/ID-10460, vol. 1, U.S. Department of Energy, Washington, DC, USA (1995).
9. H. J. Park, V.K. Dhir, “Effect of Oustside Cooling on the Thermal Behavior of a Pressurized Water Reactor Vessel Lower Head,” Nuclear Technology, vol. 100, p. 331 (1992).
10. J.E. O’Brien, G.L. Hawkes, “Thermal Analysis of a Reactor Lower Head with Core Relocation and External Boiling Heat Transfer,” AIChE Symposium Series, Heat Transfer, p.159 Minneapolis, MN, USA (1991).
11. R.E. Henry, H.K. Fauske, “External Cooling of a Reactor Vessel under Severe Accident Conditions,” Nuclear Engineering and Design, vol. 139, p. 31 (1993).
12. J.S. Kim, T.E. Jin, “Strucutural Integrity Assessment of the Reactor Pressure Vessel

under the External Reactor Vessel Lower Head," Nuclear Engineering and Design, vol. 191, p. 117 (1999).
13. T.G. Theofanous, M. Maguire, S. Angelini, T. Salmassi, "The First Result from ACOPO Experiment," Nuclear Engineering and Design, vol. 169, p.49 (1997).
14. M.M. El-Wakil, Nuclear Heat Transport, ch. 4, International Textbook Company, Scranton (1971).
15. S. Globe, D. Dropkin, Journal of Heat Transfer, vol. 81, p. 24 (1959).
16. M.S. El-Genk, C. Gao, "Transient Heat Conduction During Quenching of Downward Facing Copper and Stainless Steel Convex Surfaces," Numerical Heat Transfer Part A, vol. 29, p. 543 (1996).
17. H.J. Yoon, Kune Y. Suh, "Two Dimensional Analysis for the External Vessel Cooling Experiment," Journal of the Korean Nuclear Society, vol. 32, no. 4, p. 410 (2000).
18. L. A. Stickler, J.L. Rempe, S.A. Chavez, G.L. Thinnes, S.D. Snow, R.J. Witt, M.L. Corradini, J.A. Kos, Calculations to Estimate the Margin to Failure in the TMI-2 Vessel, appendix a, NUREG/CR-6196 TMI V(93)EG01 EGG-2733, Washington, DC, USA (1994).
19. F.B. Cheung, Y.C. Liu, Critical Heat Flux Phenomenon on a Downward Facing Curved Surface: Effect of Thermal Insulation, NUREG/CR-5534 PSU/ME-98-7321, Washington, DC, USA (1998).

Table 1 Correlations Considered in This Study

Parameter	Correlation
Natural Convection in the Molten Pool	Theofanous et al. [13]
Angular Heat Flux Distribution	Theofanous et al. [8]
Critical Heat Flux	Rouge et al. [5]

Table 2 Parameters for Case Study

Parameter	1	2	3	4
Time of Corium Relocation after Reactor Trip (s)	7200	5400	3600	
Mass Flow Rate of External Coolant (kg/s)	20	30	40	50
Initial Subcooled Condition of External Coolant (°C)	0	60		

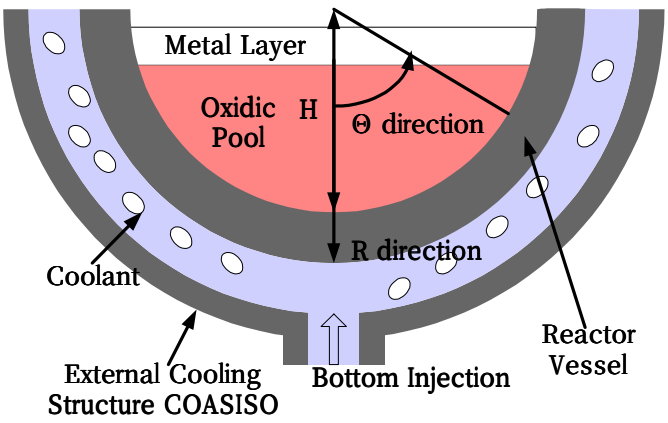

Figure 1 Schematic Diagram for COASISO

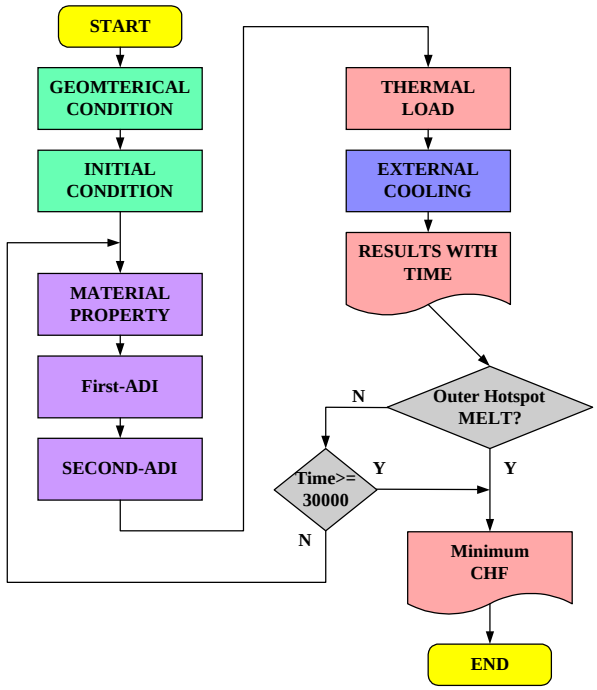

Figure 2 Flow Diagram

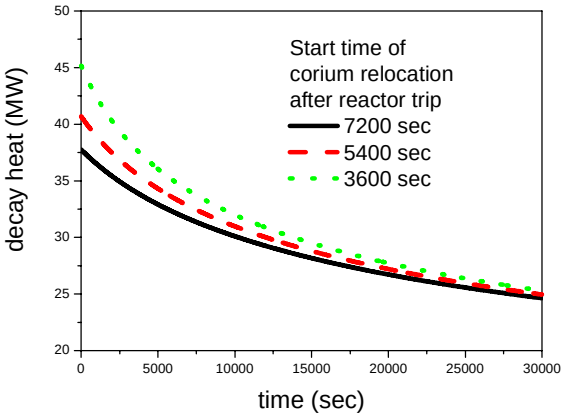

Figure 3 Decay Heat in Corium

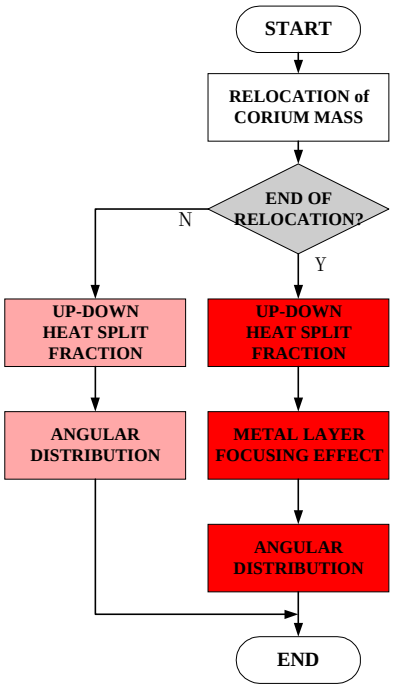

Figure 4 Flow Diagram for Thermal Load

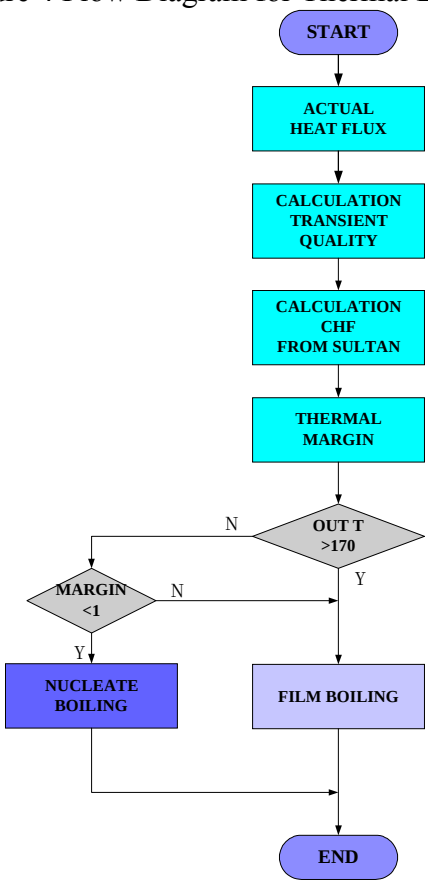

Figure 5 Flow Diagram for the Local HTC

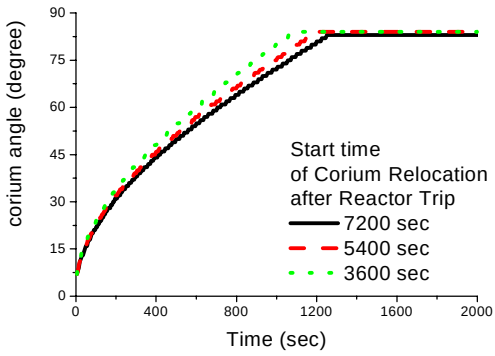

Figure 6 Corium Angle Variation with the Start Timeof Corium Relocation after Reactor Trip

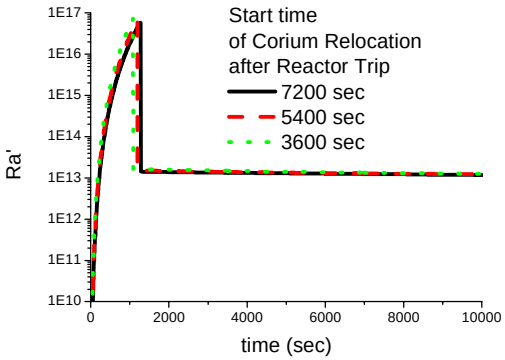

Figure 7 Ra' Variation with the Start Time of Corium Relocation after Reactor Trip

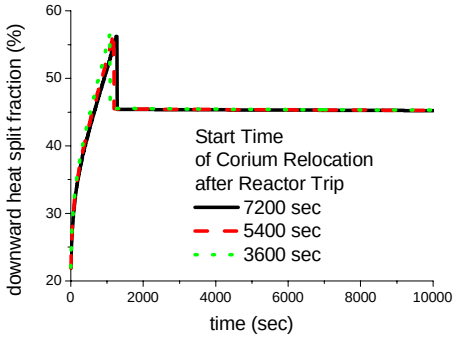

Figure 8 Heat Split Variation with the Start Time of Corium Relocation after Reactor Trip

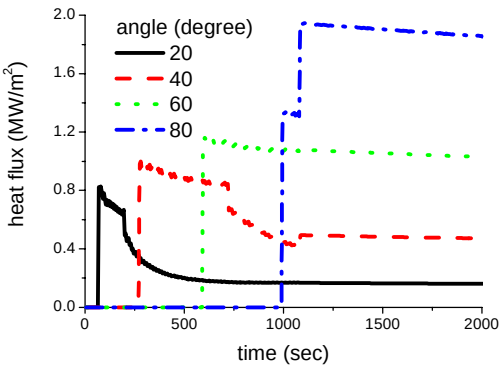

Figure 9 Initial Thermal Load in Case 342

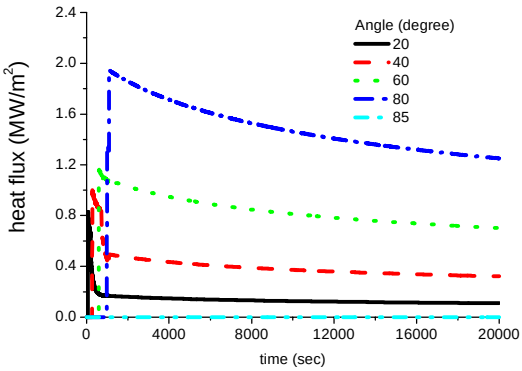

Figure 10 Thermal Load in Case 342

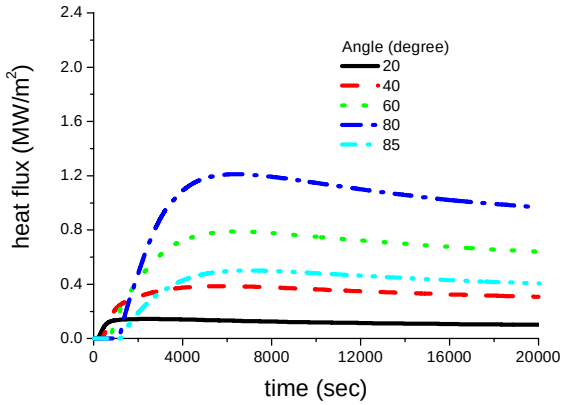

Figure 11 Outer Heat Flux in Case 342

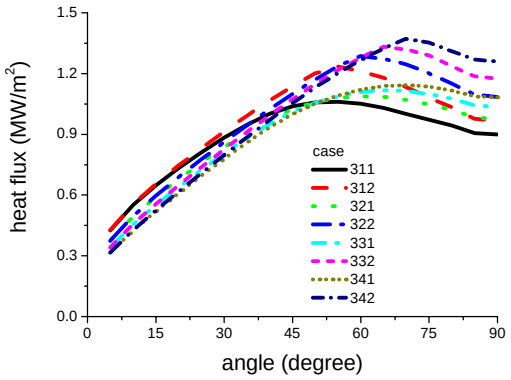

Figure 12 Angular Minimum CHF Distributions

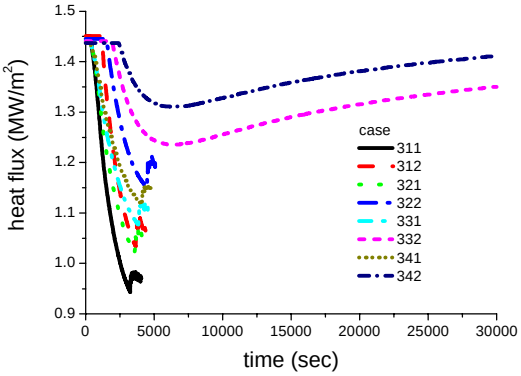

Figure 13 History of Critical Heat Flux at 80^o

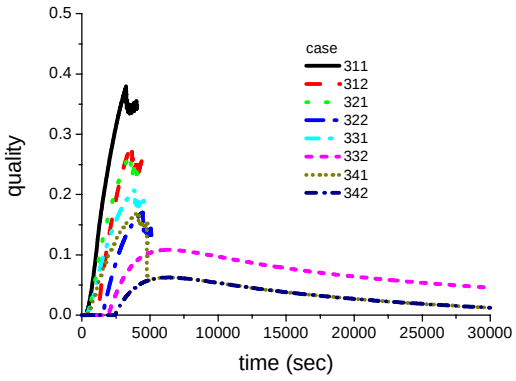

Figure 14 History of Local Quality at 80^o

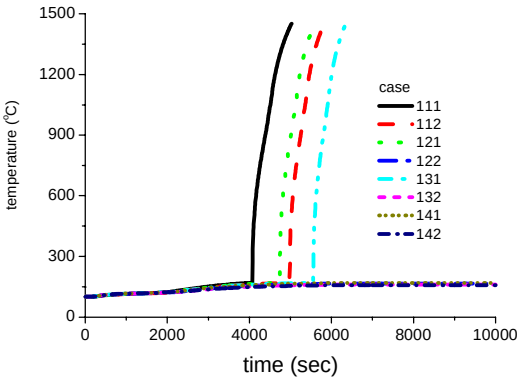

(a) 2.0 hr

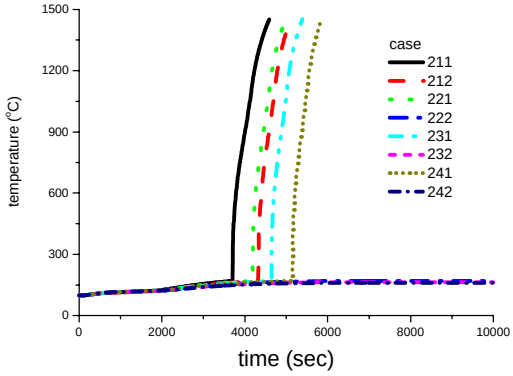

(b) 1.5 hr

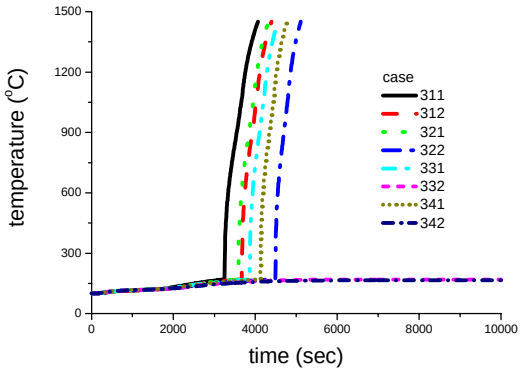

(c) 1.0 hr

Figure 15 History of Maximum Temperature of the Outer Wall